Turbulent Boundary-Layer Shock Interaction with and without Injection

E. ALZNER* AND V. ZAKKAY†
New York University, Bronx, New York

Experimental results of turbulent boundary-layer shock interaction at Mach 6 using a 10° axisymmetric wedge around an axisymmetric centerbody are presented. Static pressure, pitot pressure and total temperature profiles, wall static pressure distributions, heat-transfer distributions and optical data have been obtained. Air and hydrogen are injected to study their effects on the interaction region. Wall heat transfer and pressure distributions for different injection rates of both air and hydrogen are also presented. Detailed mappings of Mach number, pressure distributions and shock wave locations are derived for the no injection as well as the air injection case. The results show a natural boundary-layer thickness of about 0.85 inches, a separated flow region about two inches long and a pressure plateau characteristic of turbulent flow. Heat-transfer and pressure measurements indicate a relationship $q \sim p^n$ where $0.725 \leq n \leq 0.815$ over the parts of the interaction region where measurements were made. The mappings show the differences in the various distributions due to one air injection rate. Hydrogen injection verifies that considerably less injectant mass flow rate is required for similar cooling when the specific heat of the coolant is increased.

Nomenclature

L = reference length from rear of shock generator to zero reference for measuring probe position
M = Mach number
$\mathfrak{M}$ = molecular weight
N = exponent in Eq. (1)
p = pressure
q = heat-transfer rate
R = gas constant (= $\mathfrak{R}/\mathfrak{M}$)
$\mathfrak{R}$ = universal gas constant
T = temperature
U = axial velocity
x = axial coordinate
y = normal coordinate
γ = ratio of specific heat
δ = boundary layer thickness
δ^* = displacement thickness
λ = mass flow per unit area ratio, = $\rho_i U_i/\rho_e U_e$
Θ = nondimensional total temperature, = $T_0 - T_w / T_{0\infty} - T_w$
θ = momentum thickness

Subscripts

e = external to boundary layer
j = injectant
0 = stagnation value
r = reference condition
w = wall value
2 = behind the shock
∞ = freestream value

Presented as Paper 70-91 at the AIAA 8th Aerospace Sciences Meeting, New York, January 19–21, 1970; submitted March 3, 1970; revision received December 17, 1970. This work was supported by the Aerospace Research Laboratories, Office of Aerospace Research, USAF, Wright-Patterson AFB, Ohio, under contract F33615-68-C-1184, and was performed in partial fulfillment of the requirements for the Ph.D. degree of the first author, in the School of Engineering and Science of New York University.
* Assistant Research Scientist, presently Research Scientist, Advanced Technology Laboratories.
† Professor of Aeronautics and Astronautics. Associate Fellow AIAA.

I. Introduction

THE advent of hypersonic flight has given rise to complex vehicle and propulsion system configurations. In the inlet of an airbreathing propulsion system where oblique shock waves impinge on the surface, and in configurations where bow shocks interact on struts and wing surfaces, regions of boundary-layer shock interaction are prevalent. This phenomenon with the associated separation region can significantly affect the air induction system efficiency and flight characteristics of the vehicle.

Although there has been a great deal of investigation and a degree of success for laminar flow, little progress by comparison has been made for turbulent flow. Most investigations have stressed primarily pressure distributions and profile data. Furthermore the models were usually finite flat plates and quite often the turbulent boundary layer was produced by tripping a laminar layer. The inherent flaw of this tripping technique is the possibility of the relaminarization of the flow. In addition heat-transfer data was found to be lacking in most investigations, and injection or suction studies were usually performed in a preliminary manner and with a lack of heat-transfer data.

Details of the present study can be found in Ref. 1. Some of the previous more interesting studies were carried out by the following investigators. Kutschenreuter, et al.[2] did an extensive investigation using a two-dimensional model. Holden[3] studied some theoretical and experimental aspects of the interaction problem and Childs, Paynter and Redecker[4] used a "patching" technique to try to predict separation and reattachment points. The cold wall turbulent boundary layer itself was discussed by Perry and East[5] and Myring[6] dealt with the over-all interaction problem within the confines of the limitation outlined above. A good summary of heat transfer involved in the interaction phenomenon was presented by Markarian.[7]

Suction or injection can alter the pressure and heat-transfer distributions. In this connection Kutschenreuter et al.[8] and Pearson[9] experimented with wall suction while Shetz and Giltroth,[10] Peake[11] and Howell and Tatro[12] experimented with tangential injection from a rearward facing step. A more recent study of the basic interaction problem for both laminar and turbulent flow was carried out by Watson,

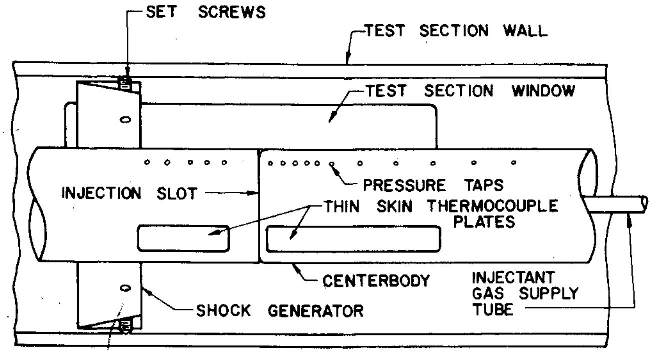

Fig. 1 Schematic shock generator and centerbody in test section.

Murphy and Rose,[13] however here again one drawback was the lack of heat-transfer data and the fact that the turbulent boundary layer was not a natural one.

The present investigation was then carried out to include heat-transfer observations, effects of injection and suction and to provide a detailed picture (mapping) of the interaction region with and without air injection.

An axisymmetric model was chosen to more closely simulate an engine inlet and to avoid the problem of side effects as in the case with finite width flat plates.

II. Experimental Investigation

The present investigation was carried out at New York University Aerospace Laboratory with the aim to 1) investigate boundary-layer shock wave interactions in an axisymmetric wind tunnel with a naturally turbulent boundary layer; 2) investigate heat transfer as well as pressure distributions; and 3) study the effect of injection of different gases on heat transfer and pressure distribution.

A. Wind Tunnel

The high Reynolds' number facility capable of producing a naturally turbulent boundary layer was used for these experiments. A description of the facility can be found in Ref. 1. One important feature of the facility is a fast acting plug valve which separates the high-pressure heater and nozzle and which allows impulsively rapid (0.1 sec) establishment of steady-state flow conditions so necessary for good heat-transfer measurements by the transient thin wall technique.

B. Model

An instrumented axisymmetric centerbody was located along the axis of the nozzle and test section, and an axisymmetric wedge shaped shock generator was mounted near the wall of the test section (Fig. 1). The centerbody is contoured along a streamline of the nozzle flow starting at the throat and reaching a constant diameter of 4.623 in. in the test section. The shock generator is an axisymmetric wedge shaped ring 3 in. long and $11\frac{5}{8}$ in. in diameter at the leading edge with a flow deflection angle of 10°.

The model was instrumented with static pressure taps and heat-transfer gauges. The heat-transfer gauges consisted of thermocouples mounted on the inner surface of 0.005-in.-thick stainless steel shim stock which was contoured to the centerbody surface shape. As pointed out earlier, heat transfer was thus measured by the transient thin wall technique by the application of a step temperature change. Since the initial slope of the temperature trace was used as a measure of the heat transfer and since the shim stock was very thin, longitudinal and lateral heat-transfer effects can be neglected.

For the injection tests, an injection slot was designed to provide injection as tangential as possible without having a rearward facing step. The slot had its minimum area at the exit resulting in sonic conditions there. Slot heights of 0.010 and 0.030 in. were used.

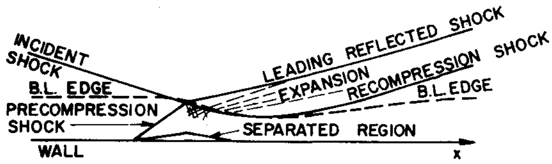

Fig. 2 Schematic of shock wave interaction region.

C. Instrumentation

A Honeywell Visirecorder multichannel recording galvenometer with a response time of less than 0.01 sec was used to record the experimentally measured pressures and temperatures. A "scanivalve" sampling valve was used for the wall pressure "scanning." A triple probe having total temperature, static pressure and pitot pressure sensors traversed the boundary layer by means of a precision traversing mechanism. Shadowgraphs and Schlieren pictures were taken to provide optical data.

D. Flowfield

The Mach 6 axisymmetric flow with a stagnation temperature of about 800°R and a stagnation pressure of about 1800 psia provided a Reynold's number of the order of 2×10^8 in the test section and led to a turbulent boundary-layer thickness, δ, of 0.85 in. The displacement thickness, δ^*, at 1800 psia is about 0.286 in. and at 900 psia is about 0.413 in. For the latter a momentum thickness, θ, of 0.029 in. was found.

E. Description of the Investigation

The experimental investigation of the turbulent boundary-layer shock wave interaction with and without injection took on the following phases.

Phase I

Conduct an investigation of the interaction with and without injection using an axisymmetric shock generator of 10°. It was also the aim in this phase to study the effect of the interaction as a result of varying; a) the location of the injection; and b) the injection mass flow rate.

Phase II

Probe in detail the interaction region without injection to obtain pressure and temperature profiles and pressure and heat-transfer distributions.

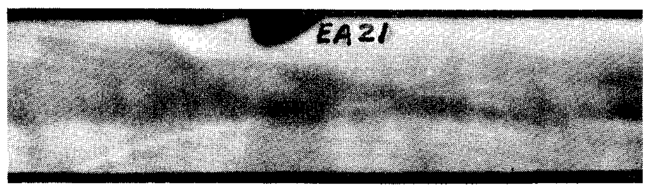

Fig. 3a Schlieren of test 21—no shock generator, λ = 0.

Fig. 3b Schlieren of test 20—shock generator, λ = 0.

Table 1 Phase I test numbers

Position	L	$\lambda = 0.0$	0.331	0.736
0	NSG	21	...	...
1	3.284	13,14	15	16
2	4.724	19,20	18	17
3	6.145	24,25	23	22

Phase III

Probe in detail the interaction region with one injection location and one injection mass flow rate using air injection to obtain profiles and distributions as those in Phase II.

Phase IV

Study the effect on the interaction region as a result of using a different injection gas (namely hydrogen instead of air).

Phase I was conducted with a stagnation pressure of about 1850 psia and a slot height of 0.010 in. while the remaining phases were run at about half the pressure and with a slot height of 0.030 in. This was done since the relatively small size of the traversing probes limited their strength as well as their rigidity. Schlierens and shadowgraphs were taken in support of the recorded data and to provide composite optical and pressure results.

III. Experimental Results

The data to be presented was nondimensionalized so that valid comparisons could be made. Pressures were normalized by the freestream stagnation pressure of each test to eliminate slight variations from test to test. Heat-transfer rates were divided by the heat-transfer rates at the same locations from a test using no shock generator and no injection. Corrections were also applied to account for the minor differences in the stagnation temperature of different tests.

A. Phase I Tests

One aim of these tests not mentioned earlier was to determine some of the basic characteristics of the turbulent boundary-layer shock wave interaction phenomenon. Some

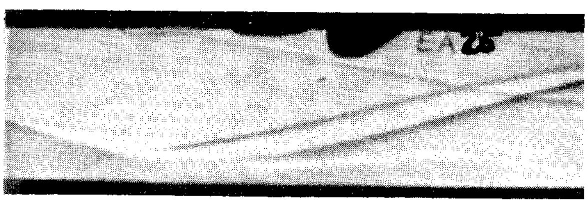

Fig. 4a Shadowgraph of test 25 ($\lambda = 0$).

Fig. 4b Shadowgraph of test 23 ($\lambda = 0.331$).

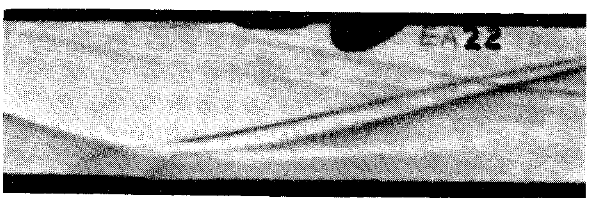

Fig. 4c Shadowgraph of test 22 ($\lambda = 0.736$).

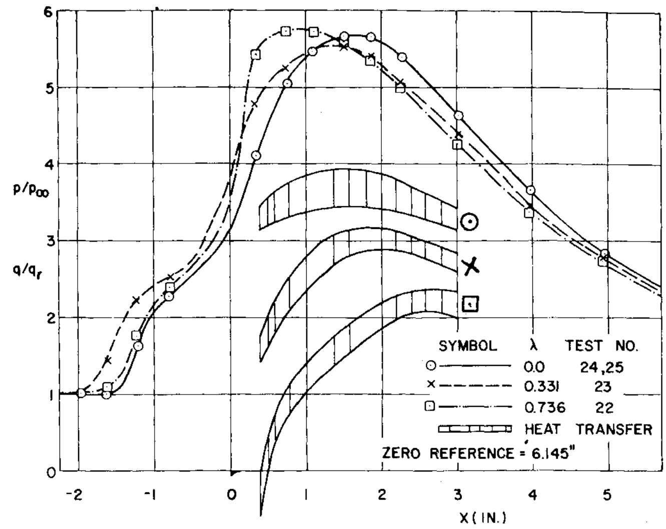

Fig. 5 Wall pressure and wall heat-transfer distributions for position 3 ($L = 6.145$; $\lambda = 0.0$; 0.331; 0.736).

of the essential features of the interaction are shown schematically in Fig. 2. Indicated are the incident shock, the separation shock (or precompression shock as it is labelled here), the leading reflected shock which is a transmitted and intensified separation shock, the expansion due to the turning of the flow and the recompression or reattachment shock.

The injection slot had three different locations with respect to the interaction region and three values of injectant mass flow rate (including no injection) at each location were tested. Table 1 provides identification of these quantities.

Test 21 was conducted with no shock generator (NSG) and no injection ($\lambda = 0.0$) and provided the reference values for heat transfer and a Schlieren of the basic Mach 6 flow. Figure 3a shows this and the edge of the boundary layer (0.85 in. thick) can be clearly seen. Also visible is the minor disturbance from the injection slot. The relative weakness of this disturbance can be evaluated by comparison with Fig. 3b which is a Schlieren of a no injection test. The shock system is of the greater strength than the injection slot disturbance. The expansion from the rear of the shock generator is also visible just upstream of the window disturbance. Thus, the 10° flow deflection is effective only over a finite region and results downstream of the expansion impingement must be ignored.

For positions 1 and 2, injection slot located upstream of and at the separation shock, respectively, the cooling was not as effective in the peak heating region and no data for these are

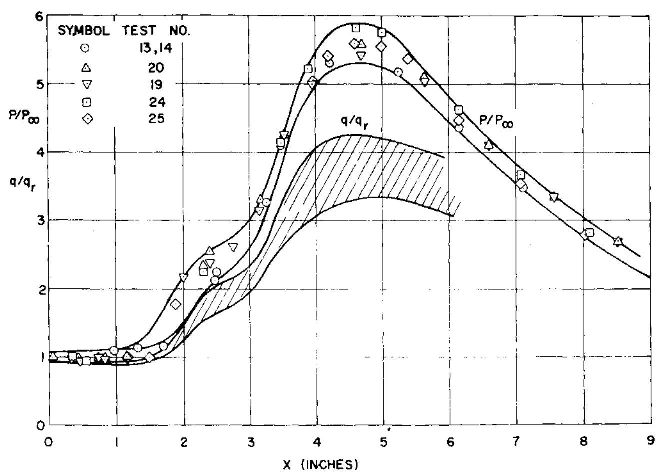

Fig. 6 Composite wall pressure and heat-transfer distributions for $\lambda = 0$.

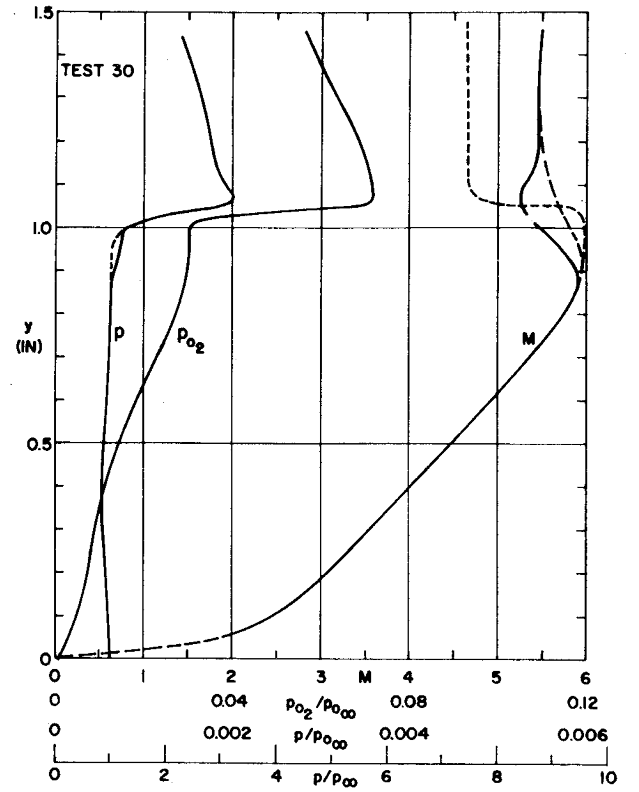

Fig. 7 Static pressure, pitot pressure and derived Mach number profiles at $x = 1.28$, Phase II.

presented. For full details of all shadowgraphs and profiles the reader is referenced to Ref. 1. Certain shifts of the shock system take place due to injection and only one set of comparison shadowgraphs will be presented. This is shown in Fig. 4a, b and c which is for position 3. The results for the pressure and heat-transfer distributions are also presented for this position.

Figure 5 presents the pressure and heat-transfer distributions for position 3 (injection slot located near the reattachment point) with the three injection mass flow rates. The plateau shift reflects the separation shock relocation and the motion of the peak results from the reattachment shock movement (refer also to Figs. 4a, b and c).

The heat-transfer reduction obtained with the injection in the region near the reattachment point was much more pronounced than for the other positions since cooling was provided in the peak heating region. In all of these tests the basic pressure distribution prevailed and little effect on reducing the separated region was found. The main benefit was the reduction of heat transfer to the surface. The negative

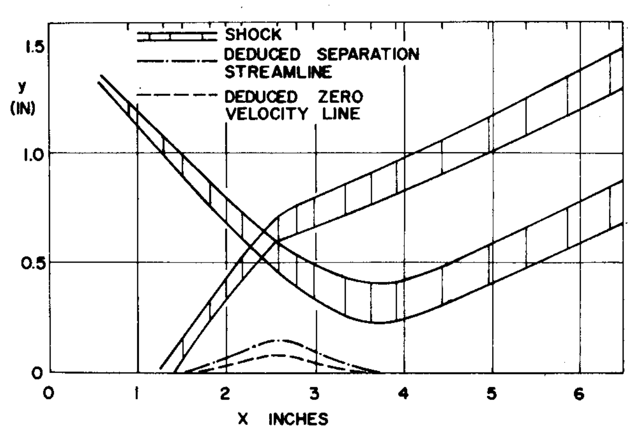

Fig. 8 Shock locations as derived from maximum pressure gradient locations, Phase II

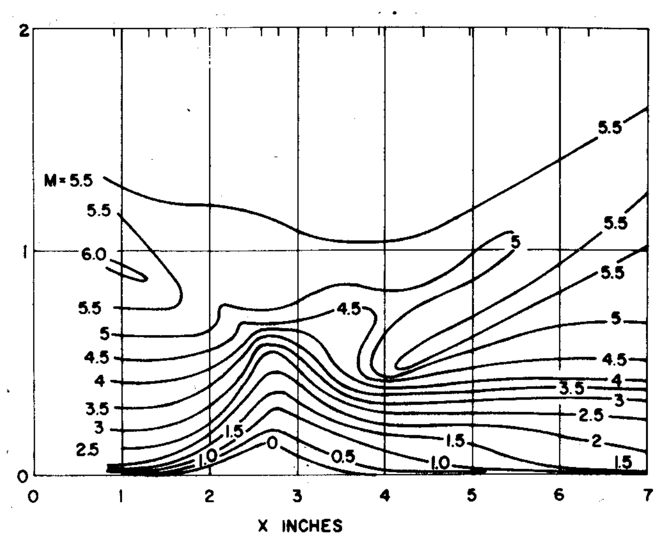

Fig. 9 Mappings of constant Mach number lines, Phase II.

values of heat transfer arise due to the throttling effect of the injection slot. In order to exert a greater influence on the flow it was decided to enlarge the slot from 0.010 – 0.030 in. for the subsequent tests.

Figure 6 is a composite of the no injection tests (tests 13, 14, 19, 20, 24 and 25) and a band width is drawn about the pressure and heat-transfer data. A comparison of the two curves reveals a correlated relationship

$$q \sim p^n \tag{1}$$

where $0.725 \leq n \leq 0.815$ over the range of data. This agrees well with results presented in Ref. 7.

B. Phase II Tests

The aim of this phase of tests was to provide a detailed mapping of the flowfield derived from probing the flow with static pressure, pitot pressure and total temperature probes. Profiles were taken at 18 x stations (only 7 temperature profiles were useful). The reference length L is 5.617 in. Phase II tests were conducted at a stagnation pressure of about 950 psia. Figure 7 presents the profiles upstream of the interaction and a slight effect due to the injection slot can be seen in the static pressure profile, which, near the wall, is not quite constant. The dashed line on the Mach number profile represents the theoretically predicted Mach number behind a 10° wedge oblique shock. Figure 7 also reveals the laminar na-

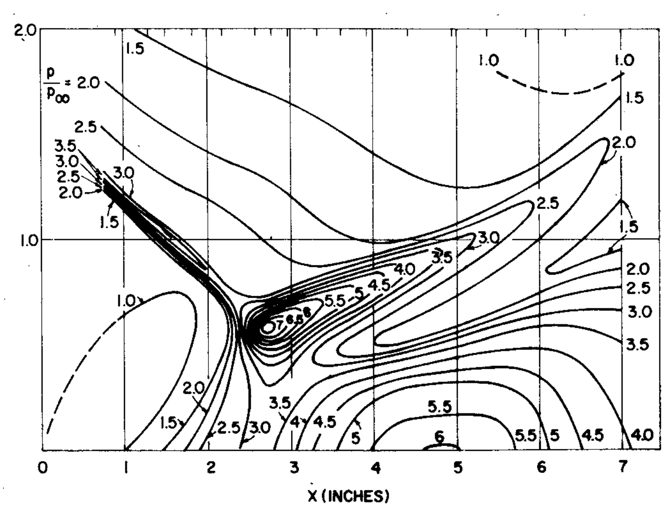

Fig. 10 Mapping of constant static pressure lines, Phase II

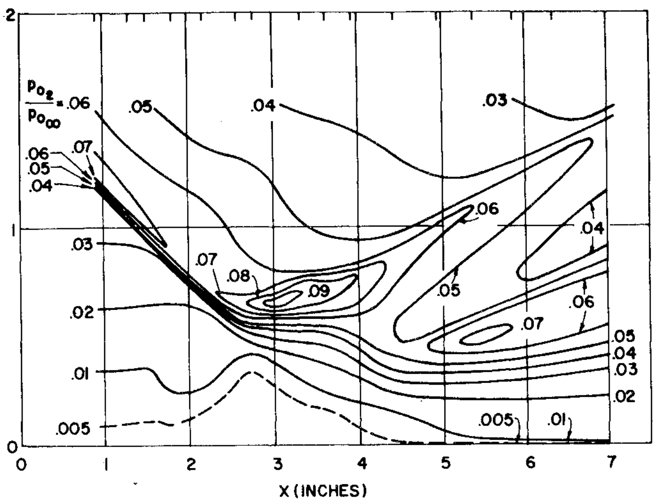

Fig. 11 Mapping of constant pitot pressure lines, Phase II.

ture of the static probe[14] which is reflected in a slight plateau ahead of the sharp gradient and the drop in pressure beyond the peak. This laminar nature results in the incorrect determination of the Mach number when the probe traverses the shock.

The locations of the maximum gradients can be used to trace the movement of the shock system. Figure 8 depicts the shock wave locations as determined from the locations of the maximum gradients and has the y coordinate stretched by a factor of 2.5. This was done so that the mappings of Mach number, static pressure and pitot pressure could be more clearly represented. These mappings are presented in Figs. 9, 10 and 11, respectively. The Mach number mapping (Fig. 9) gives a clear indication of the separated flow region since the zero Mach line is obviously embedded in the separated flow region. Figure 10 reveals regions of maximum pressure gradients where the isobars are closest and again the shock wave locations can be deduced. The maximum pressure in the whole interaction region occurs behind the intersection of the incident and separation shocks. This is in keeping with theoretical intuition. Figure 11 gives good indications of maximum gradient (shock wave) locations.

Figure 12 presents the nondimensional total temperature profiles $\Theta = (T_0/T_w)/(T_{0\infty} - T_w)$ and the derived static temperature and velocity profiles. From these results it is of interest to plot U/U_∞ against Θ and see how this curve fits either the Crocco relation

$$\Theta = U/U_\infty \tag{2}$$

or

$$\Theta = (U/U_\infty)^2 \tag{3}$$

Figure 13 presents this comparison graph and it is observed that the present data essentially fits between them except near U/U_∞ and Θ of unity where Θ has an overshoot. For a cold wall the curve would fit closer to Eq. (3) and the overshoot would disappear based on results of Ref. 5.

The separated region was defined more accurately by two techniques. A total pressure probe was traversed through the separated region facing both upstream and downstream. Where the two values were equal, and in fact equal to the static pressure, there was the zero velocity line. This also allowed an approximate determination of the separation and reattachment points. In order to obtain better locations of these two points, ink was allowed to ooze out of a pressure tap and its maximum upward travel marked the separation point and the point where excess ink was allowed to wash away dried ink marked the reattachment point.

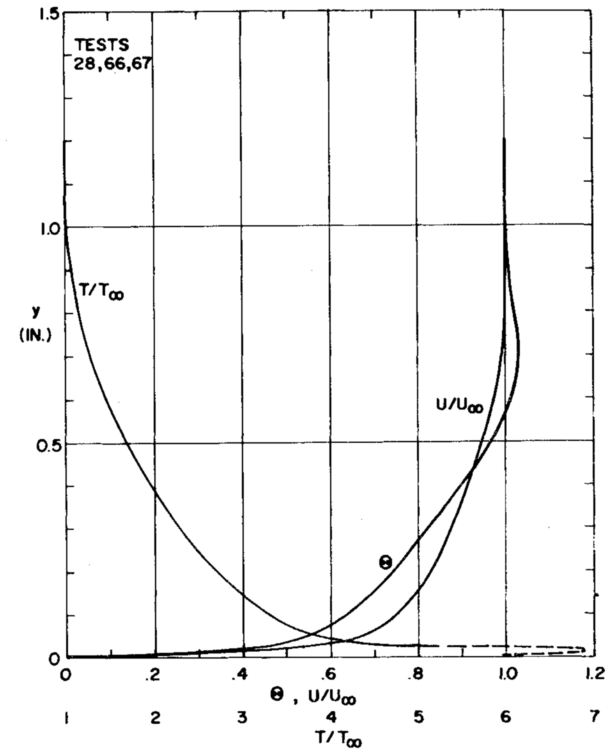

Fig. 12 Total temperature and derived static temperature and axial velocity profiles at x − 0.89, Phase II.

C. Phase III Tests

This phase was equivalent to Phase II except that air was injected in the separated region approximately one half inch ahead of the reattachment point determined in Phase II. The injection had a value of $\lambda = 1.26$. The reference length L for Phase III was 5.395 in. and this must be added to the x coordinate for each profile for an absolute location behind the rear of the shock generator. The difference in L between Phase II and Phase III is 0.222 in. and this difference was accounted for in presenting the mappings for Phase III.

As in Phase II, maximum pressure gradients imply shock wave locations and Fig. 14 presents the shock locations with the expanded y scale for comparison. An additional large gradient region having a concave-down shape as a result of the injection. Also the separated region is split in two and now eliminated with this particular slot configuration.

The Mach number distribution shown in Fig. 15, is altered primarily in the vicinity of the injection slot and downstream

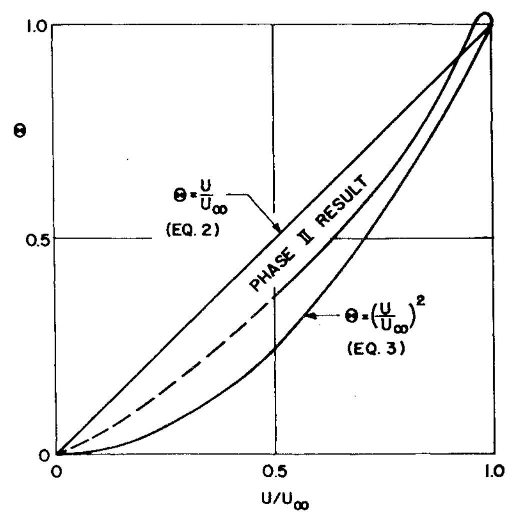

Fig. 13 Comparison of initial velocity—total temperature profile to linear and quadratic relationship, Phase II.

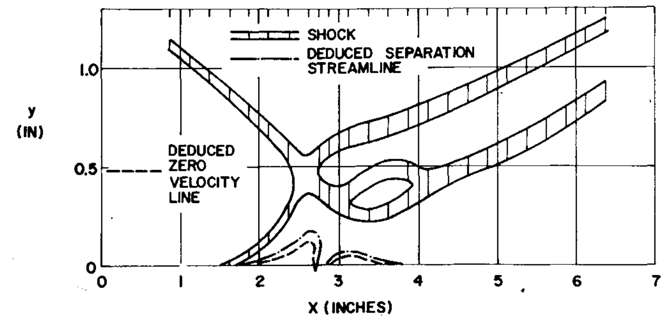

Fig. 14 Shock locations as derived from maximum pressure gradient locations (Phase III).

of this position. A small separation bubble is present downstream of the injection slot ending at the original reattachment point. This is obviously due to the nontangency of the injection. The static pressure distribution presented in Fig. 16 shows effects in the same domains with peak pressure again occurring behind the intersection of the incident and separation shocks. Figure 17 presents the pitot pressure map and only slight changes are observed in the same regions downstream of the injection slot.

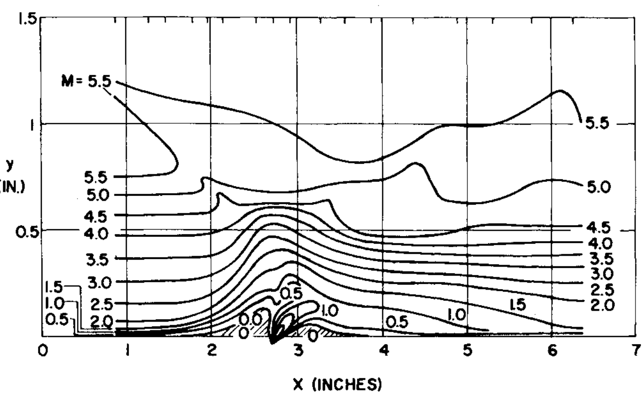

Fig. 15 Mapping of constant Mach number lines, Phase III.

A comparison of wall pressure distribution with and without injection is shown in Figure 18. It was found that wall pressures measured within the static probe near the wall were slightly higher than wall static measurements and this was reasoned due to the blockage effect that a probe has, especially near the wall.

D. Phase IV Tests

The final phase of this experimental investigation was designed to provide information about the effect of varying the injection mass flow rate and the effect of changing the molecular weight of the injectant. Five different injection rates for each injectant air and hydrogen were called for. The range of hydrogen injection rates was designed to give the same approximate range of cooling as the air injection. Table 2 summarizes the tests.

Table 2 Values of λ for phase III

Gas	λ	Test no.
Air	0.205	124
	0.535	125
	1.260	129
	1.620	126
	2.080	127
	2.740	128
No injection	0.000	130
H_2	0.045	131
	0.056	132
	0.086	133
	0.113	134
	0.140	135
	0.187	139
Suction	<0	136

Figure 19 presents the comparisons of pressure distributions for the various injection rates for air and Fig. 20 presents this comparison for hydrogen. Hydrogen injection was performed to study the effect of injecting a gas of different physical properties and in particular because of the large differences of molecular weight and specific heat as compared to air. It is of interest to note the strong effect hydrogen injection has on the plateau and how the larger injection rates almost eliminate any sign of a plateau.

One additional important set of data was obtained during Phase IV and that was the effect of various λ's on wall heat transfer. Figure 21 presents the heat-transfer comparisons of air injection with no injection. Interestingly enough, for larger rates ($\lambda \geq 1.26$), there appears to be evidence of separated flow behind the injection slot, since the effective cooling is less immediately behind the slot than somewhat further downstream. Of course, this separation was found in Phase III and is no surprise. It is likely that for smaller values of λ, there is also a separated region but this cannot be stated with certainty without further testing.

The equivalent result for hydrogen injection is shown in Fig. 22. Much greater cooling is obtained near the slot since hydrogen has a much greater specific heat. Some evidence of separation behind the slot is present as indicated by the inflected curves. Actually hydrogen is a more effective coolant in two respects. First, as mentioned, the specific heat is higher, hence, the same heat can be carried by a smaller mass

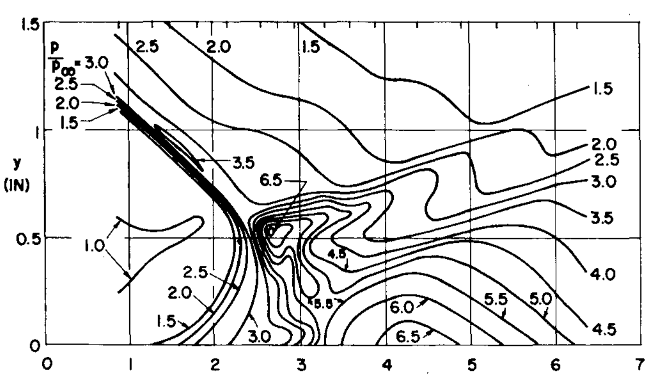

Fig. 16 Mapping of constant static pressure, Phase III.

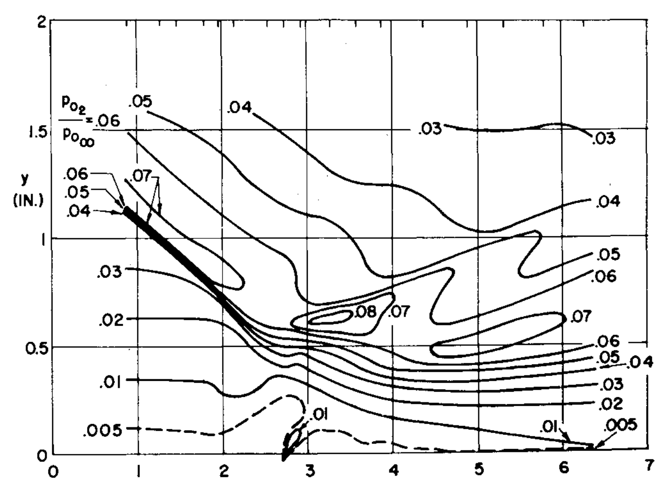

Fig. 17 Mapping of constant pitot pressure, Phase III.

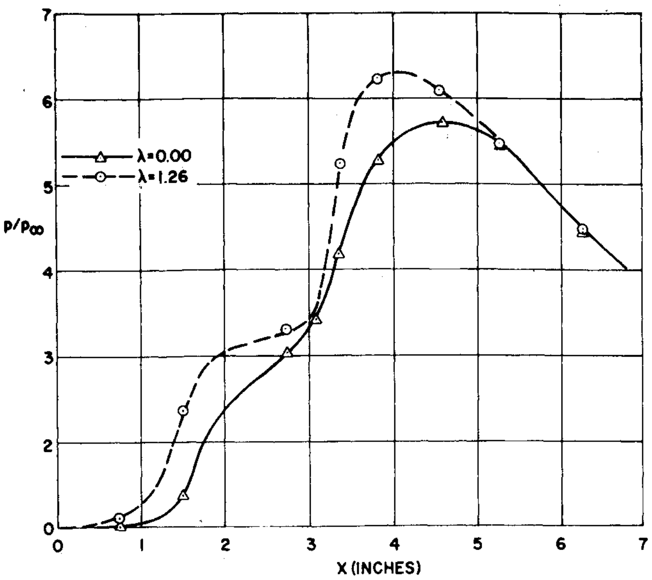

Fig. 18 Comparison of wall static measured wall pressure distributions for λ = 0 and λ = 1.26.

flow. Second, since the slot exit is sonic and since the throttling produces the same static temperature at the slot exit (because $\gamma = c_p/c_v = 1.4$ for both), the velocity for hydrogen is greater by the ratio of the square root of the molecular weights, i.e.,

$$U = M\{\gamma RT\}^{1/2} = M\{\gamma(\mathcal{R}/\mathfrak{M})T\}^{1/2} \tag{4}$$

$$U_{H2}/U_{\text{air}} = \{\mathfrak{M}_{\text{air}}/\mathfrak{M}_{H2}\}^{1/2} \approx 4 \tag{5}$$

Thus the heat-transfer coefficient, which is dependent on the velocity, is higher for hydrogen immediately behind the slot. So we see that hydrogen not only carries more heat away but also picks it up faster. Suction tests showed no observable changes; hence they will not be discussed.

F. Reliability of Results

Repeatability of results was quite good as determined from comparisons of several repeat tests. Probe interference was minimal since the probes were quite small compared to the separated region and comparison of static probe pressure at the wall to wall static pressure where the error would be largest turned out to show only small differences. The accuracy of measurements combined with the degree of repeatability led to the conclusion that pressure results are accurate to within about 5% and heat-transfer results to within about 10%. The heat-transfer results are less accurate since slopes of curves instead of absolute values are measured on the data traces. This more than doubles the possible reading error and is reflected in the larger tolerance.

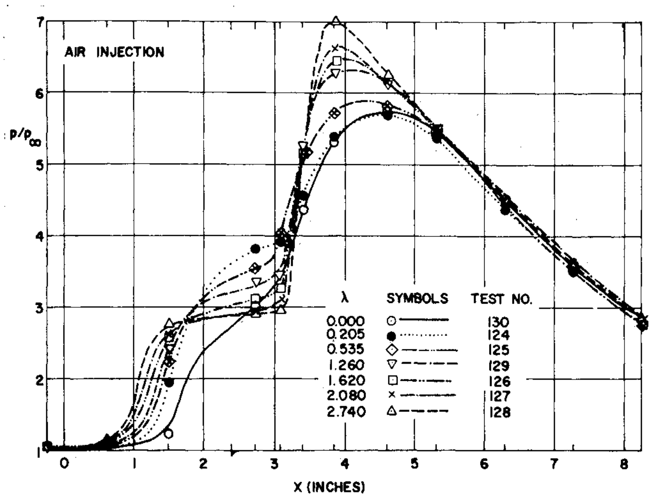

Fig. 19 Wall pressure distributions for air injection studies, Phase IV.

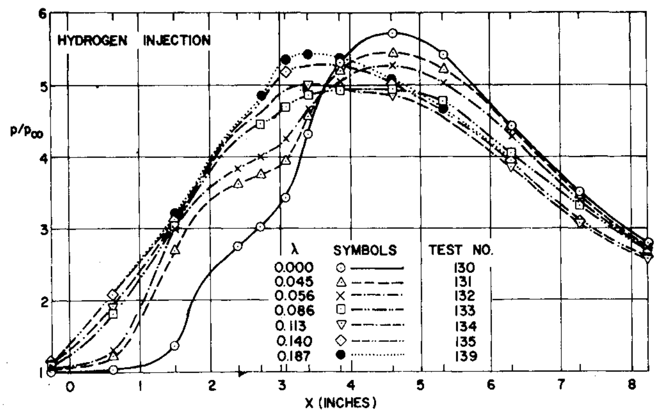

Fig. 20 Wall pressure distributions for hydrogen injection studies, Phase IV.

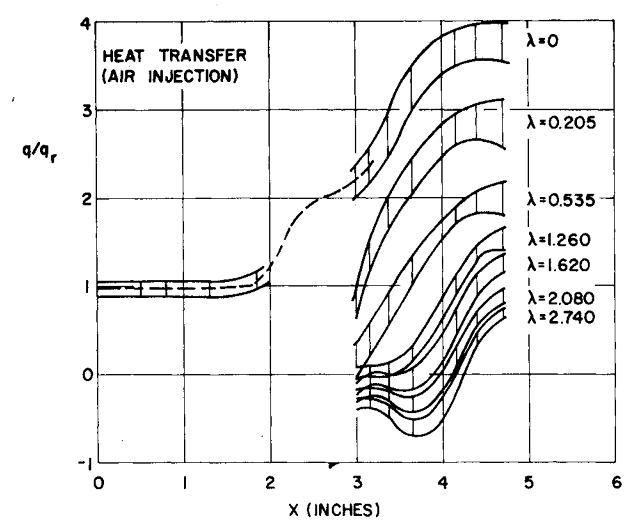

Fig. 21 Heat-transfer distributions for air injection, Phase IV.

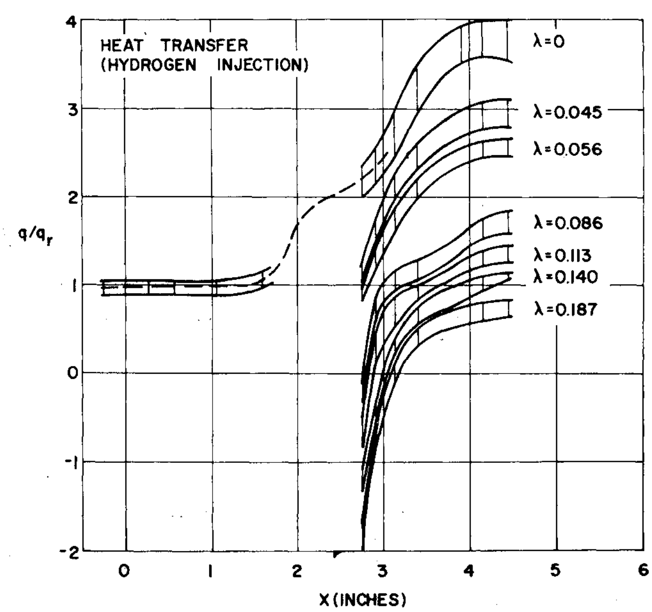

Fig. 22 Heat-transfer distributions for hydrogen injection, Phase IV.

IV. Conclusion

From the large amount of data obtained in these experiments, excellent mappings of pressure and Mach numbers for injection and no injection were generated and a good comparison of the two flows can be made. Due to the large boundary-layer thickness excellent optical and profile data with little or no probe interference was obtained.

From the mappings and detailed probing of the separated regions the following picture of the flow was deduced. The incident shock produces a sharp unfavorable pressure gradient which leads to reverse flow and separation of the boundary layer. From the region of the separation point the separation shock emanates and passes through and is intensified by the incident shock. The flow behind the separation shock is away from the wall while the flow behind the incident shock is towards the wall. The net result is a turning of the flow back to the wall with an expansion emanating from the maximum height of the separated flow region. The flow now is towards the wall and must be turned parallel to the wall again at the reattachment point. The turning gives rise to the reattachment or recompression shock.

Results showed that significant cooling can be achieved if the injection is suitably located. Hydrogen injection provided data about the effect of varying the molecular weight and specific heat of the injectant. Much less hydrogen than air was required for the same amount of cooling. Due to the large effect of hydrogen injection on the pressure plateau it would be of interest to conduct a series of tests to generate a flow mapping for hydrogen injection.

References

[1] Alzner, E. and Zakkay, V., "Turbulent Boundary Layer Shock Interaction with and without Injection," NYU Rept. 69-24, 1970, New York Univ., New York, ARL Rept. 70-0092, 1970, Aeronautical Research Lab., Tullahoma, Tenn.

[2] Kutschenreuter, P. H., Jr., Brown, D. L., Hoelmer, W., et al., "Investigation of Hypersonic Inlet Shock-Wave Boundary Interaction," Pts. I and II, AFFDL-TR-65-36, March 1965, Air Force Flight Dynamics Lab., Wright-Patterson Air Force Base, Ohio.

[3] Holden, W. S., "Theoretical and Experimental Studies of Separated Flows Induced by Shock Wave-Boundary Layer Interaction," *AGARD Conference Proceedings No. 4, Separated Flows*, Pts. 1 and 2, May 1966.

[4] Childs, M. E., Paynter, G. C., and Redecker, E., "The Prediction of Separation and Reattachment Flow Characteristics for Two-Dimensional Supersonic and Hypersonic Turbulent Boundary Layers," *AGARD Conference Proceedings, No. 4, Separated Flows*, Pts. 1 and 2, May 1966.

[5] Perry, J. H. and East, R. A., "Experimental Measurements of Cold Wall Turbulent Hypersonic Boundary Layers," *AGARD Conference Proceedings No. 30, Hypersonic Boundary Layers and Flow Fields*, May 1968.

[6] Myring, D. P., "The Interaction of a Turbulent Boundary Layer and a Shock at Hypersonic Mach Numbers," *AGARD Conference Proceedings No. 30, Hypersonic Boundary Layers and Flow Fields*, May 1968.

[7] Markarian, C. F., "Heat Transfer in Shock Boundary Layer Interaction Regions," NWC TP 4485, Nov. 1968, Naval Weapons Center, Chica Lake, Calif.

[8] Kutschenreuter, P. H., Zurschmeide, R. L., and Surber, L. E., "An Investigation of Shock Wave-Boundary Layer Intersection with Suction," ASRMDF TM 61-30, Jan. 1962.

[9] Pearson, L. W., "Effects on Slot Suction on Turbulent Boundary Layer Separation," AIAA Paper 67-197, New York, 1967.

[10] Shetz, J. A. and Gilroth, H. E., "Tangential Slot Injection in Supersonic Flow," AIAA Paper 67-198, New York, 1967.

[11] Peake, D. J., "The Use of Air Injection to Prevent Separation of the Turbulent Boundary Layer in Supersonic Flow," C.P. 890 (AD 805480), 1966, Ministry of Aviation, Aeronautical Research Council.

[12] Howell, G. A. and Tatro, R. E., "Tangential Fluid Injection for Control of Shock-Boundary Layer Interaction," AIAA Paper 66-656, Colorado Springs, Colo., 1966.

[13] Watson, E., Murphy, J., and Rose, W., "Investigation of Laminar and Turbulent Boundary Layers Interacting with Externally Generated Shock Waves," TN D-5512, Nov. 1969, NASA.

[14] Liepmann, H. W. and Roshko, A., "Elements of Gasdynamics," Wiley, New York, 1957, p. 146.